On reversible bonding of hydrogen molecules on platinum clusters

Szarek, Pawel; Urakami, Kousuke; Zhou, Chenggang; Cheng, Hansong; Tachibana, Akitomo

THE JOURNAL OF CHEMICAL PHYSICS **130**, 084111 (2009)

On reversible bonding of hydrogen molecules on platinum clusters

Paweł Szarek,[1] Kousuke Urakami,[1] Chenggang Zhou,[2] Hansong Cheng,[3] and Akitomo Tachibana[1,a)]
[1]*Department of Micro Engineering, Kyoto University, Kyoto 606-8501, Japan*
[2]*Institute of Theoretical Chemistry and Computational Materials Science, China University of Geosciences, Wuhan 430074, China*
[3]*Air Products and Chemicals, Incorporated, 7201 Hamilton Boulevard, Allentown, Pennsylvania 18195-1501, USA*

(Received 3 August 2008; accepted 19 December 2008; published online 26 February 2009)

The local reactivity of hydrogenated platinum clusters (Pt clusters) has been studied using the regional density functional theory method. We observed that antibond orbitals constitute the preferable binding site for hydrogen molecules H_2. Those sites are characterized by lowered electronic chemical potential and strong directionality and exhibit electrophilic nature. The platinum-dihydrogen (Pt–H_2) sigma complexes were formed only by occupation of the lowest electronic chemical potential sites associated with Pt–H antibonds (σ_{PtH}^{*}) in saturated platinum clusters. The formation of sigma complexes caused mutual stabilization with the *trans* Pt–H bond. Such activated H_2 molecules on Pt clusters in a sense resemble heme-oxygen (heme-O_2) complex with interaction strength greater than physisorption or hydrogen bonding but below chemisorption strength. © *2009 American Institute of Physics*. [DOI: 10.1063/1.3072369]

I. INTRODUCTION

Hydrogen is expected to substitute for fossil fuel and to be a cost effective, renewable, and clean alternative energy source. Yet the mass production and storage of hydrogen turn out to be an essential problem. The technical targets of these tasks were specified by the U.S. Department of Energy (DOE).[1] Thus far utilized methods and materials cannot sufficiently fulfill the expectations.[1–4] The classes of new materials are studied.[4–10] However their properties, although promising, are still not in the target zone. The characterization of the nature and strength of hydrogen interaction with promising materials is fundamental for a successful development of satisfactory novel applicable technologies.

Among a variety of tested materials, metal clusters attract particular attention. The hydrides are long known as one of the stabilizing ligands of metal clusters. Some features of these "macro atoms," such as high surface area to volume ratio, their electronic structures, and high density of edges, corners, and other reactive centers, leading to greatly improved catalytic activity and aggressive chemical reactivity, make them potentially important in hydrogen economy.

The simple way of understanding the properties of solid matter, especially concerning the irregularities of structure, is to study the clusters containing an increasing number of atoms. These nanodimensional materials are an intermediate state between molecules and bulk solid, and they may share properties of both, resulting in very peculiar physical and chemical properties compared to macroscale. The dominant role is played by effects related to the quantization of energy for the electrons in solids with great reductions in particle size.

The properties of transition metals, particularly platinum possessing high resistance to chemical attack, excellent high-temperature characteristics, and stable electrical properties, make them desirable in industrial applications. Moreover platinum is an important catalyst in hydrogenation and dehydrogenation reactions. However its application in fuel cell implies additional restrictions regarding the amount of platinum required (and thus cost). Even though, the study of Pt materials is of primary importance, providing understanding of hydrogen chemistry and thus contributing to the development of cheaper yet effective materials.

II. THEORY

The energy density at the macroscopic level can be used to express energy stored in the capacitor (for electric fields) or energy stored in the inductor (for magnetic fields). The field energy (energy density) in chemical systems at the atomic or molecular level is related to electromagnetic waves. The electromagnetic waves are associated with both the electric and magnetic fields that play a role in the transport of energy. The corresponding energy density of the electromagnetic field might be obtained within the regional density functional theory (RDFT) method[11–18] as the invariance of electronic stress tensor due to nonrelativistic limit of the rigged QED (RQED) energy density.[12,15]

The RDFT method[18,19] allows the assigning of electronic energy density to electron density in the chemical reaction system as a unique functional of electron density. The quantum mechanical nature of electrons that can tunnel from a region R to neighboring regions allows the replacement of all Hamiltonians (originally for each region in Onsager's local equilibrium theory) by one density functional Hamiltonian that covers the system as a whole.[11] The regional partitioning is based on a coordinate representation of the density

a)Electronic mail: akitomo@scl.kyoto-u.ac.jp.

matrix.[11] The integration with respect to Cartesian coordinates r_i and spin coordinates σ_i is first divided into

$$\int \prod_i d^3\vec{r}_i d\sigma_i = \int d^3\vec{r}_1 \int d\sigma_1 \prod_{i\neq 1} d^3\vec{r}_i d\sigma_i \tag{1}$$

and finally into regional partitions,

$$\int d^3\vec{r}_1 = \sum_R \int_R d^3\vec{r}_1. \tag{2}$$

The integration of energy density over a small region (extended to an infinitely small region) gives local electronic energy contribution to global electronic energy E. Integration over the whole space leads to the total energy E of the system. The local energy density constitutes very small partial contribution to the total electronic energy in the same sense that electron density is a small portion of the total electron number.

The electronic stress tensor [Eq. (3)][12,16] that reflects internal distortion of electron density and the intensity of total internal forces within a molecule (which results in relevant flow of electric charge through a particular region), in local picture, allow us to study chemical reactivity.[15,20] The electronic stress tensor, as a second rank tensor, is given by a 3×3 matrix,

$$\langle \hat{\vec{\tau}}^S(\vec{r})\rangle = \begin{bmatrix} \tau^S_{xx}(\vec{r}) & \tau^S_{xy}(\vec{r}) & \tau^S_{xz}(\vec{r}) \\ \tau^S_{yx}(\vec{r}) & \tau^S_{yy}(\vec{r}) & \tau^S_{yz}(\vec{r}) \\ \tau^S_{zx}(\vec{r}) & \tau^S_{zy}(\vec{r}) & \tau^S_{zz}(\vec{r}) \end{bmatrix} \overset{\text{diag}}{\rightarrow} \begin{bmatrix} \tau^{S11}(\vec{r}) & 0 & 0 \\ 0 & \tau^{S22}(\vec{r}) & 0 \\ 0 & 0 & \tau^{S33}(\vec{r}) \end{bmatrix}, \tag{3}$$

$$\tau^{S11}(\vec{r}) \le \tau^{S22}(\vec{r}) \le \tau^{S33}(\vec{r}), \tag{4}$$

with matrix elements

$$\tau^{Skl}(r) = \frac{\hbar^2}{4m}\sum_i^{\text{occ}} \nu_i \left[\psi_i^*(\vec{r}) \frac{\partial^2 \psi_i(\vec{r})}{\partial x^k \partial x^l} - \frac{\partial \psi_i^*(\vec{r})}{\partial x^k}\frac{\partial \psi_i(\vec{r})}{\partial x^l} + \frac{\partial^2 \psi_i^*(\vec{r})}{\partial x^k \partial x^l}\psi_i(\vec{r}) - \frac{\partial \psi_i^*(\vec{r})}{\partial x^l}\frac{\partial \psi_i(\vec{r})}{\partial x^k}\right]. \tag{5}$$

The principal stresses characterize compressive (negative) and tensile (positive) tendencies of charge density in space. The atomic core regions are associated with highly compressive stresses, while tensile stress, present in the form of a "spindle structure"[16] of an interatomic region, indicates a covalent bond. The local contribution to electronic energy [$\varepsilon^S_\tau(\vec{r})$, Eq. (6)] is given by half of the trace over the eigenvalues of the electronic stress tensor,[14]

$$\varepsilon^S_\tau(\vec{r}) = \frac{1}{2}\sum_k \tau^{Skk}(\vec{r}), \quad E = \int d^3\vec{r}\varepsilon^S_\tau(\vec{r}). \tag{6}$$

The energy density partitioning scheme[11,18,19,21,22] utilized in RDFT leads to three related energy components derived from the same density matrix. The total energy density is decomposed into the potential and interelectron potential energy densities and the kinetic energy density. The latter plays a particularly important role in the characterization of space of chemical systems. The relevant kinetic energy density ($n_T(\vec{r})$ [Eq. (7)] and $\psi_i(\vec{r})$ are natural orbitals, and ν_i is the occupation number of $\psi_i(\vec{r})$) is nonpositively defined and divides the real space of chemical moieties into electronic drop [$R_D: n_T(\vec{r})>0$] and atmosphere [$R_A: n_T(\vec{r})<0$] regions separated by an interface surface [$S: n_T(\vec{r})=0$],[12]

$$n_T(\vec{r}) = -\frac{\hbar^2}{4m}\sum_i^{\text{occ}} \nu_i [\psi_i^*(\vec{r})\Delta\psi_i(\vec{r}) + \Delta\psi_i^*(\vec{r})\psi_i(\vec{r})]. \tag{7}$$

The surface S of $n_T(\vec{r})$ (defining the turning point for electrons) encloses the molecular regions of reactants and defines the boundaries of separate chemical species since in the R_A region the classical movement of electrons is denied.

Under the linear approximation, the ratio of local energy density and corresponding electron density [understood as very small regional contributions to total values $(\partial E/\partial N)$] gives the electronic chemical potential at a particular point in space,[23]

$$\mu_R = \left(\frac{\partial E_R}{\partial N_R}\right) \Leftrightarrow \frac{\varepsilon^S_{\tau AB}(\vec{r})}{n_{AB}(\vec{r})}, \tag{8}$$

$$E_{AB} = \int d^3\vec{r}\varepsilon^S_{\tau AB}(\vec{r}), \quad N_{AB} = \int d^3\vec{r} n_{AB}(\vec{r}). \tag{9}$$

The electronic chemical potential represents the effective potential experienced by associated electron density. The chemical potential also measures the tendency of particles to diffuse (a function of spatial location). Particles diffuse from regions with high chemical potential to regions with low chemical potential. This makes the gradient of chemical potential an effective electric field. The electron density is stationary where the gradient of chemical potential is zero (all forces are balanced). The Gibbs chemical potential μ_G is defined as a change in electronic energy E as a function of electron number N,

$$\mu_G = \left(\frac{\partial E}{\partial N}\right)_{S,v}. \tag{10}$$

The Sanderson[24] principle of electronegativity equalization implies that chemical potential should be constant for all electrons for ground state electron density. However, it was proven that inhomogeneity of $\rho(r)$ is associated with inhomogeneity of regional chemical potentials μ_R.[18,19,21] The measurements of the work function of metals as a function of crystallographic planes[25,26] could be used to demonstrate the chemical potential inequality principle.[11] The gradient of chemical potential exists in irreversible thermodynamics of Onsager[27] and Bardeen[28] where each region has its own Hamiltonian. The inequality of regional chemical potentials, under the condition of global chemical equilibrium, evolves from the quantum mechanical interference effect between electrons in any region and electrons in regions in complementary space. The distribution of electrons treated with DFT Hamiltonian possesses coherence, and only one electronic Hamiltonian covering the whole system can be used.

In global chemical equilibrium, the quantum mechanical law of mass action reads

$$\mu_G = \mu_R + \sum_{R'(\neq R)} \alpha_{R'R}, \tag{11}$$

where, except for the regional chemical potential, the $\alpha_{R'R}$ term appears, which measures the quantum mechanical interference effect ($\sim \partial E_R / \partial N_{R'}$). Dropping the interference term leads to Sanderson's principle of electronegativity equalization,

$$\mu_R = \mu_{R'} = \mu_{R''} = \cdots = \mu_G. \tag{12}$$

The total electronic force [Eq. (13)], defined within RQED, is composed of Lorentz force and tension force.[12,14,16,29] For a stationary state of charged particles, the total force becomes zero; thus tension is balanced by Lorentz force at every point in space. The expectation value of tension force density operator, given as the divergence of the stress tensor density operator [Eq. (14)], at the stationary state between chemically bonded atoms can locally vanish at the Lagrange point,[23]

$$\langle \hat{\vec{\tau}}^S(\vec{r}) \rangle + \langle \hat{\vec{L}}^S(\vec{r}) \rangle = 0, \tag{13}$$

$$\begin{aligned} \hat{\tau}^{Sk}(\vec{r}) &= \partial_l \hat{\tau}^{Skl}(\vec{r}) \\ &= \frac{\hbar^2}{4m} \sum_i^{\text{occ}} \nu_i \left[\psi_i^*(\vec{r}) \frac{\partial \Delta\psi_i(\vec{r})}{\partial x^k} - \frac{\partial \psi_i^*(\vec{r})}{\partial x^k} \Delta\psi_i(\vec{r}) \right. \\ &\quad \left. + \frac{\partial \Delta\psi_i^*(\vec{r})}{\partial x^k} \psi_i(\vec{r}) - \Delta\psi_i^*(\vec{r}) \frac{\partial \psi_i(\vec{r})}{\partial x^k} \right]. \end{aligned} \tag{14}$$

This peculiar stationary point of charge density in the interatomic region provides reliable characteristics of bond properties.[20,23] The nonclassical bond order measures[23] were based on electronic properties calculated at the Lagrange point. b_ε, the energy density bond order [Eq. (15)], and b_μ, the chemical potential bond order [Eq. (16)], were introduced,

$$b_\varepsilon = \frac{\varepsilon^S_{\tau AB}(\vec{r}_{\text{Lagrange}})}{\varepsilon^S_{\tau \text{HH}}(\vec{r}_{\text{Lagrange}})}, \tag{15}$$

$$\begin{aligned} b_\mu &= \frac{b_\varepsilon}{(n_{AB}(\vec{r}_{\text{Lagrange}})/n_{\text{HH}}(\vec{r}_{\text{Lagrange}}))} \\ &= \frac{\varepsilon^S_{\tau AB}(\vec{r}_{\text{Lagrange}})}{n_{AB}(\vec{r}_{\text{Lagrange}})} \cdot \left(\frac{\varepsilon^S_{\tau \text{HH}}(\vec{r}_{\text{Lagrange}})}{n_{\text{HH}}(\vec{r}_{\text{Lagrange}})} \right)^{-1}, \end{aligned} \tag{16}$$

which are the respective quantities at the Lagrange point of the particular bond relative to H_2 molecule as a reference value calculated at the same level of theory.

The hybrid variational-perturbational interaction energy decomposition scheme[30] with counterpoise correction[31] was applied to obtain the MP2 interaction energy components [Eq. (17)], where $\Delta E^{(1)}_{\text{el}}$ is the electrostatic energy, $\Delta E^{(1)}_{\text{ex}}$ stands for exchange energy arising from the overlap of charge distributions and Pauli exclusion principle, $\Delta E^{(R)}_{\text{del}}$ is the delocalization component associated with the relaxation of electronic clouds upon interaction, and ΔE_{corr} is the second-order correlation energy. The sum of successive components gives interaction energy at gradually increasing levels of theory,

$$\begin{aligned} &\Delta E = \Delta E^{(1)}_{\text{el}} + \Delta E^{(1)}_{\text{ex}} + \Delta E^{(R)}_{\text{del}} + \Delta E_{\text{corr}} \\ &\text{——————MP2——————} \\ &\text{——————SCF————} \\ &\text{————HL————} \\ &\text{——EL——} . \end{aligned} \tag{17}$$

The two-body interaction energy density[23] calculated as a difference in energy densities of dimer (AB) and monomers (A and B, without relaxation) in the dimer centered basis set [Eq. (18)],

$$\Delta\varepsilon_{AB}(\vec{r}) = \varepsilon_{AB}(\vec{r}) - (\varepsilon_A(\vec{r}) + \varepsilon_B(\vec{r})), \tag{18}$$

shows regions where electronic energy becomes lower due to the interaction; thus attractive and repulsive trends of charge density between atoms of the considered system are visualized.

TABLE I. The rms of atom positions of dmol3 (Ref. 32) and Gaussian 03 optimized hydrogenated platinum clusters.

Cluster	Pt atoms (rms)	H atoms (rms)	All atoms (rms)
Pt_2H_{10}	0.024	0.628	0.584
Pt_3H_{12}	0.010	0.098	0.089
Pt_4H_{16}	0.020	0.095	0.086
Pt_5H_{20}	0.041	0.258	0.236
Pt_7H_{28}	0.120	0.245	0.226
Pt_8H_{30}	0.039	0.076	0.071
Pt_9H_{34}	0.097	0.193	0.178

III. CALCULATION METHODS

Recently reported hydrogenated Pt clusters[32] were further studied here using the RDFT method.[11–17] The structures were reoptimized by GAUSSIAN 03 (Ref. 33) calculations employing the generalized gradient approximation of exchange-correlation energy with Wang and Perdew[34] (PW91PW91) parametrization in the standard 6-31G** basis set for hydrogen atoms and LanL2DZ (Ref. 35) 18-electron effective core potential for Pt atoms. Although the double precision numerical basis set corresponds to the Gaussian 6-31G** basis set,[36–39] obtained structures were essentially different in particular cases. The rms of atom positions of initial[32] and GAUSSIAN 03 reoptimized structures are shown in Table I. These differences in geometries (predominantly related to H atoms) result from the presence of polarization functions on H atoms since optimalization using D95/LanL2DZ or 6-31G/LanL2DZ (H/Pt atoms, respectively) leads to almost identical geometry-like initial structures.[32] The 6-31G** basis set was employed due to the inclusion of polarization functions in basis sets, which is important for calculating the equilibrium geometries[40] particularly when studying processes involving hypervalent molecules, $3c/2e$ interactions, σ-complexes, and agostic interactions.[41–43] Moreover the difference in geometries might be related to small energetical barriers between local minimum structures owning to very

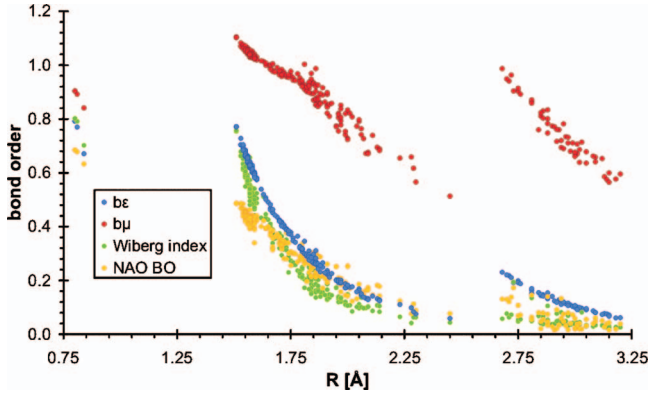

FIG. 1. (Color) Change in energy density (b_ε) and chemical potential (b_μ) bond orders with bond length. The NBO bond orders are also shown for reference.

low activation energies for H_2 chemisorption.[32] The vibrational frequencies were calculated to confirm obtaining of true minimum structures. The energy density calculations were done with the RDFT program package[44] using electron wave functions from Gaussian calculations. The visualizations of molecular structures and energy density isosurfaces were done using PYMOL (Ref. 45) and VMD (Ref. 46) programs.

IV. RESULTS AND DISCUSSION

The electronic properties of Pt clusters under full saturation are now discussed. We will focus on the GAUSSIAN 03 structures since all properties (except for the presence of σ-bonded dihydrogen species) are shared also by initial structures.[32]

A. Bond order analysis

The RQED bond orders show redistribution/dissipation of energy in a molecule and indicate bond strength in terms of energy density associated with the stationary point of electron density between atoms. The relevant point is the stress energy density flow stagnation point between atoms since starting from the Lagrange point, the energy density gets lower while moving forward a nucleus. Figure 1 [and Fig. S1 (Ref. 47)] shows the relation between bond orders and bond lengths. The bonds in the range of about 1.5–2.5 Å correspond to Pt–H bonds, while those above this range correspond to Pt–Pt bonds and those around 0.8 Å correspond to H–H bonds. The bond types can be easily recognized from b_ε or b_μ dependency on interatomic distance. Moreover b_μ allows us to distinguish between terminal two-center ($2c$) bonds from multicenter ($>2c$, like $3c/2e$) electron deficient

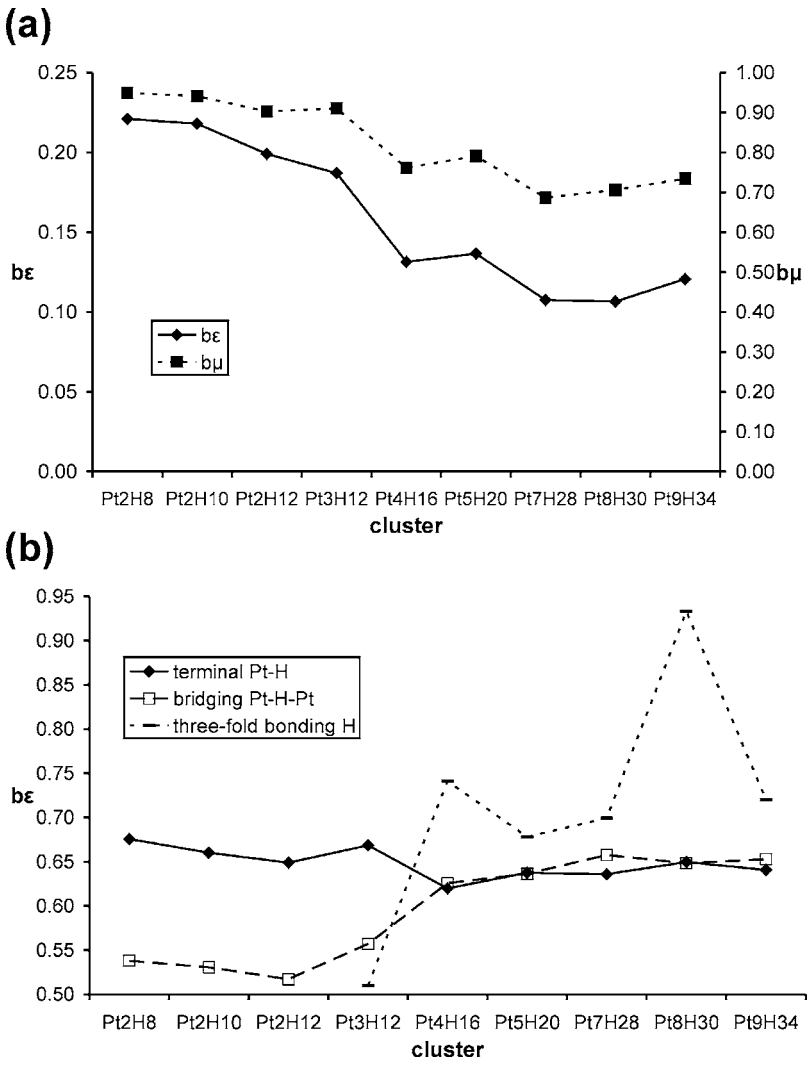

FIG. 2. The statistically average bond orders of (a) Pt–Pt bonds (b_ε and b_μ) and (b) Pt–H bonds (b_ε only) with increasing cluster size. In the case of $3c/2e$ bridging Pt(1)–H–Pt(2) bonds, the b_ε indices of Pt(1)–H and Pt(2)–H bonds were first summed, and the statistical average over "total" is shown; similarly for threefold bonding hydrogens, the statistical average over sums of bond orders of the three Pt–H bonds involved is shown.

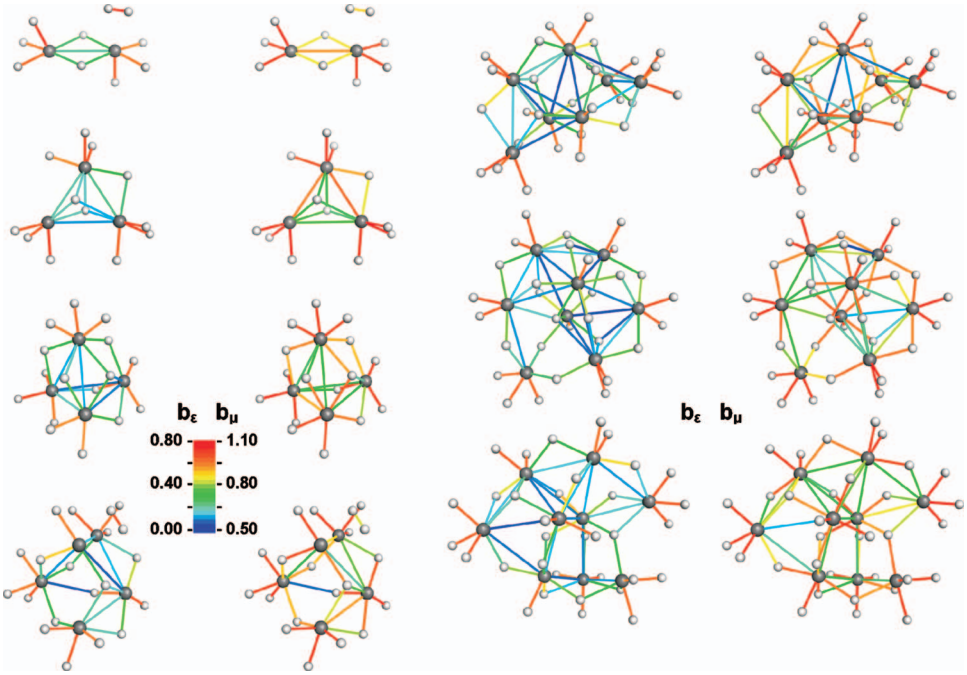

FIG. 3. (Color) The bond orders (b_ε, left column, and b_μ, right column) of bonds with the Lagrange point. The color of bond corresponds to the bond order according to scale. Pt atoms are represented as gray spheres and H atoms in white.

Pt–H bonds. The smooth trend changes around $R=1.9$ Å because the gradient of b_μ for multicenter bonds is greater than that for two-center bonds. The terminal Pt–H bonds have the greatest average strength and the most effective electric potential (measured by b_μ). The b_ε- and b_μ-bond orders correlate very well with interatomic distance. The correlation coefficients for b_ε- and b_μ-bond orders are similar or better than those of the Wiberg index (b_W) and natural atomic orbital (NAO) overlap weighted bond orders (b_{NAO}) (Ref. 33) for Pt–H (b_ε:−0.96, b_μ:−0.98, b_W:−0.93, and b_{NAO}:−0.96) and Pt–Pt (b_ε:−0.98, b_μ:−0.97, b_W:−0.55, and b_{NAO}:−0.64) bonds.

Figure 2 presents average bond order dependency on cluster size. The average Pt–Pt bond strength decreases with increasing cluster size and hydrogen loading. In general, bigger clusters also have weaker terminal Pt–H bonds; however the b_ε-bond order exhibits a slightly increasing tendency in clusters Pt_5 to Pt_9. The Pt–H–Pt, $3c/2e$ bonds are stronger in larger clusters ($b_{\mathrm{Pt-H-X}}=b_{\mathrm{Pt-H}}+b_{\mathrm{H-X}}$). The bond order indices of adsorbed H_2 molecules in Pt_2H_{10}, Pt_2H_{12}, and Pt_5H_{20} clusters are smaller than those in an isolated H_2 molecule (by definition, 1.0); thus the corresponding bond strength is weaker and the associated chemical potentials are higher. Figure 3 shows optimized structures, bonding pattern, and bond orders in Pt clusters. The tables listing all bond orders, as well as structures with atom numbering, can be found in supplementary materials (Table S1 and Fig. S2).[47]

The bridge, threefold, and fourfold bonding of hydrogen atoms might be explained in terms of bond orders and natural bonding orbital (NBO) analysis.[48,49] The structure, b_ε-bond orders, and atom identifiers of the Pt_3H_{12} cluster are shown in Fig. 4. According to the NBO analysis, the $3c/2e$ bridging H atom is bonded via the donor-acceptor interaction between hydrogen's [H(11)] s-orbital and σ_{PtH}^*-antibonds [of terminal Pt(2)–H(7) and Pt(3)–H(4) bonds, with $s_{\mathrm{H}}\rightarrow\sigma_{\mathrm{PtH}}^*$ 95.5 and 134.4 kcal mol^{-1} of NBO second-order perturbation theory stabilization respectively]. Simultaneously the backward interaction comes from σ_{PtH} orbitals with leading stabilizations, from σ_{PtH} backdonation to the s-orbital of bridging hydrogen, of 15.2 and 24.6 kcal mol^{-1}, respectively. In accordance with estimated stabilizations, the Pt(3)–H(11) bond strength (measured by b_ε) is higher than that of Pt(2)–H(11), and Pt(3)–H(4) strength is lower than that of the Pt(2)–H(7) bond. Similarly the threefold bonded hydrogen atoms are stabilized in two ways ($s_{\mathrm{H}}\rightarrow\sigma_{\mathrm{PtH}}^*$ and $\sigma_{\mathrm{PtH}}\rightarrow s_{\mathrm{H}}$) of interactions, where H(6) is stabilized by 72.8 kcal mol^{-1} [Pt(1)–H(8)], 59.3 kcal mol^{-1} [Pt(3)–H(10)], and 49.3 kcal mol^{-1} [Pt(2)–H(5)] through the $s_{\mathrm{H}}\rightarrow\sigma_{\mathrm{PtH}}^*$ donation and by 14.6 kcal mol^{-1} [Pt(3)–H(10)], 13.8 kcal mol^{-1} [Pt(1)–H(8)], and 9.0 kcal mol^{-1} [Pt(2)–H(5)] through $\sigma_{\mathrm{PtH}}\rightarrow s_{\mathrm{H}}$ backdonation, while H(15) is stabilized by 79.7 kcal mol^{-1} [Pt(1)–H(9)], 73.8 kcal mol^{-1} [Pt(3)–H(14)], and 24.8 kcal mol^{-1} [Pt(2)–H(12)] through $s_{\mathrm{H}}\rightarrow\sigma_{\mathrm{PtH}}^*$ and by 16.5 kcal mol^{-1} [Pt(3)–H(14)], 14.7 kcal mol^{-1} [Pt(1)–H(9)], and 3.6 kcal mol^{-1} [Pt(2)–H(12)] through the $\sigma_{\mathrm{PtH}}\rightarrow s_{\mathrm{H}}$ interaction. Relevant stabilizations are reflected by b_ε, which shows the lowest strengths for Pt(2)–H(6) and Pt(2)–H(15) bonds and the highest for

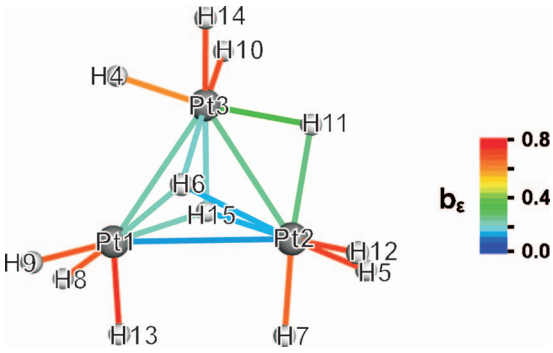

FIG. 4. (Color) The b_ε-bond order and atom numbering in Pt_3H_{12} cluster.

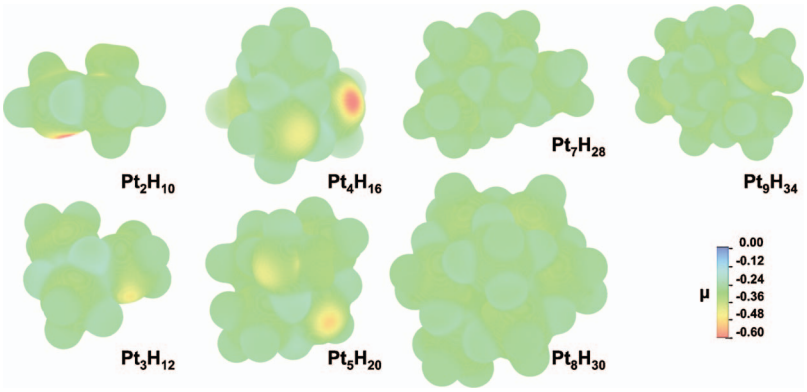

FIG. 5. (Color) Electronic chemical potential mapped on zero kinetic energy density isosurfaces.

Pt(2)–H(5) and Pt(2)–H(12). It was previously shown that hydrogen is capable of forming multicenter bonds in solids.[50–54] In the Pt_8H_{30} cluster, an atypical "fourfold" bonded H atom (four Lagrange points related to the Pt–H bonds) has been found. Such high coordination numbers for hydrogen are rare but have been reported for clusters.[54] The similar $s_H \rightarrow \sigma_{PtH}^*$ stabilizing interactions were determined [with major stabilizations of 75.5 kcal mol^{-1} Pt(4)H(37), 60.7 kcal mol^{-1} Pt(8)H(25), and 21.9 kcal mol^{-1} Pt(5)H(20) and almost equivalent contributions of 8.8 kcal mol^{-1} Pt(1)H(26) and 8.0 kcal mol^{-1} Pt(1)H(17) antibonds]. However major backdonations occurred from σ_{PtH}-bonds [62.6 kcal mol^{-1} Pt(4)H(37) and 39.1 kcal mol^{-1} Pt(8)H(25)] and from Pt lone pairs [21.4 kcal mol^{-1} Pt(5) and 15.5 kcal mol^{-1} Pt(1)]. b_ε shows the strongest bonding through the Pt(4)–H(38)–Pt(8) center associated with donor-acceptor cooperative interactions, indicating that involvement of σ_{PtH}^* and σ_{PtH} orbitals (for retrodative stabilization) results in stronger bonding of H atom than engaging σ_{PtH}^* and Pt lone pair. Recently it was shown that the antibonding orbitals on metal centers are sensed by the hydrogen atom as they were nonbonding.[55] The calculated stretching frequencies of Pt–H(38) bonds (994.9–1306.7 cm^{-1}) are lower than those of two-center Pt–H bonds (~2100 cm^{-1}).

B. The RQED energy density and MO analysis

Figure 5 presents chemical potential (μ) mapped on interface surfaces of kinetic energy density around Pt clusters. The regions of higher chemical potential around hydrogen atoms are associated with reduced electron density. However there also appear electron density deficient regions with lower chemical potential near surface exposed Pt atoms. These regions occur only in small clusters (up to five Pt atoms) and are not found on the interface surface of larger clusters.

The Pt–H bonds are characterized by the presence of spindle structure,[16] which indicates covalent interaction (the largest eigenvalue of stress is shown in Fig. S3,[47] and the corresponding eigenvector has been omitted for the sake of clarity). The regions of lower electronic chemical potential on the interface surface in proximity of Pt atoms coincide with nonspindle structure arisen tensile stress regions, as a result of strong electric potential of poorly shielded Pt nucleus (marking strengthened acceptor properties of σ_{PtH}^* of *trans* Pt–H bond and lone pair donating property). The electronic chemical potential is the effective potential experienced by electrons. The low μ means poor shielding and strong electric potential of nucleus. Therefore regions of low electronic chemical potential are "electrophilic" centers (where the electronic energy is very favorable). Contrary regions of higher chemical potential can be recognized as "nucleophilic," relatively to other parts of the molecule that will favor deflection of electron density to neighboring regions with lower μ.

We had looked closer to these spots of lower chemical potential in $Pt_2H_{n=8,10,12}$ clusters and found that these are reactive regions able to stabilize H_2 molecule ligands via synergistic σ-bond interactions. However, due to its nature (as discussed below), these can also be the electrophilic centers responsible for poisoning of Pt that can be corroded by cyanides, halogens, sulfur, and caustic alkalis. Under low saturation a H_2 coordination leads to H–H bond breaking and formation of H–Pt–H hydrides, which agrees with one of the possible reaction pathways of H_2 side-on cleavage on Pt.[32,56] Supported further by chemical potential redistribution on bare Pt clusters, where on-top binding sites on Pt show moderate lower chemical potential [figures in supporting data, Fig. S4 (Ref. 47)] associated with low electron density and tensile stress resulting from the withdrawal of electronic charge from lone pairs. However upon high saturation, H_2 molecules symmetrically bind to Pt clusters and remain dimerized. Figure 6 compares properties of $Pt_2H_{n=8,10,12}$ clusters. The H_2 coordination or insertion depends on the relative strengths of Pt–H and H–H bonds. The dihydrogen ligand b_ε-bond order is higher than any geminal or vicinal Pt–H bond, while the b_μ index is similar to that of $3c/2e$ Pt–H–Pt bridging bonds. After H_2 coordination on Pt, the nonspindle structure tensile stress diminishes and only residual positive stresses remain between Pt and dihydrogen's H atoms (a prospindle structure). Simultaneously electronic chemical potential on the interface surface around Pt–H_2 becomes high. Due to the similarity of chemical potentials of electrons of dihydrogen ligand H–H and Pt–Pt bonds, the concerning Pt–Pt bonds are likely to be inserted with bridging hydrogen.

The H–H ligand bond lengths (~0.81 Å) are found to be slightly elongated relative to "free" H_2. Pt–H_2 distances are long (~1.92 Å) relative to Pt–H terminal (~1.58 Å) and bridging (~1.86 Å) bonds but are in a typical range (1.8–2.3 Å) for σ-complex interactions.[51,52] The calculated interaction energy (Table II) also agrees with estimated usual

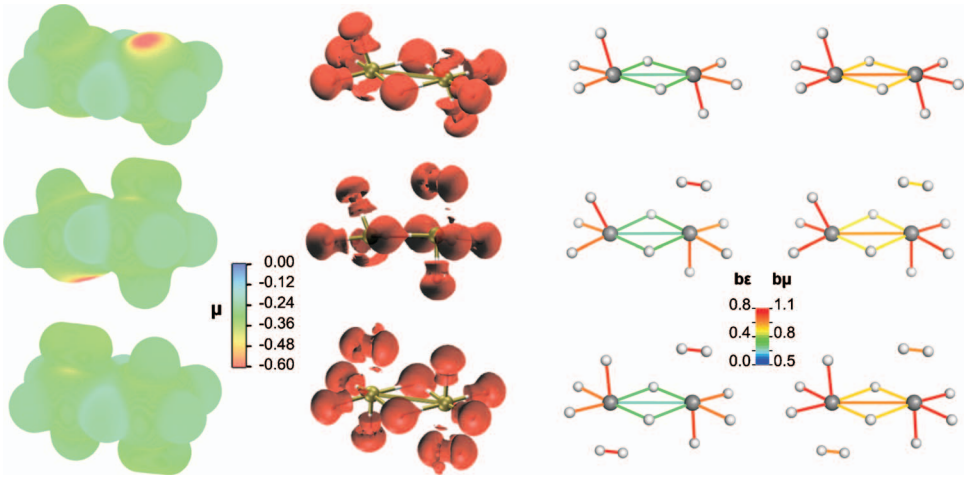

FIG. 6. (Color) Electronic properties of $Pt_2H_{n=8,10,12}$ clusters. From left to right, electronic chemical potential, largest eigenvalue of stress tensor, and b_ε- and b_μ-bond orders.

stabilization of 10–20 kcal mol^{-1}.[57–60] The highest occupied molecular orbital–lowest unoccupied molecular orbital (HOMO-LUMO) separation energies, listed in Table III, show that from Pt_2H_8 to Pt_2H_{12} reactivity of the cluster decreases as H_2 occupies low-μ sites and the relevant MO energy gap increases. Following Koopmans' theorem,[61] the increasing HOMO-LUMO gap might be associated with greater hardness of a molecule. Along with increasing HOMO-LUMO gap, the increase in the average value of local chemical potential displayed on the cluster surface is observed due to the covering of low-μ sites by H_2 ligands.

The orbitalwise analysis provided information on the MOs with the greatest contribution to $b\varepsilon$-bond order of the H–H bond. The shapes of these orbitals are presented in Fig. 7 and Fig. S5,[47] where they indicate the interaction of *d*-type orbitals of Pt and the σ-bond of H_2. In all cases relatively low energy valence electron molecular orbitals are involved in the coordination of the H_2 ligand. The natural bond order analysis of Pt_2H_{12} showed lowered occupancy (1.846 96*e*) of H_2 σ-bond and synergistic donation into the in-plane Pt–H σ^*-antibond orbital (yielding 52.4 kcal mol^{-1} of stabilization estimated from NBO second-order perturbation theory). The delocalization results in slight elongation of Pt–H bond *trans* to dihydrogen (1.53 versus 1.51 Å in Pt_2H_8). Backdonation occurs from *d* Pt lone pair to $\sigma_{HH}{}^*$-antibond orbital (8.4 kcal mol^{-1} stabilization). The b_ε-bond order shows that the relevant Pt–H bond has significantly decreased strength compared to the corresponding bond in Pt_2H_8 (or to free *trans* Pt–H bond on the second Pt atom in Pt_2H_{10}). However binding H_2 at both sites strengthens the Pt–H as well as the H–H bonds, associated with limited σ-donation and backdonation. The calculated interaction energy density (Fig. 8) shows lowering of energy (stabilization due to compression) in Pt–H_2 and *trans* Pt–H bonding regions and rise (destabilization due to expansion) in the Pt lone pair orbital, connected with migration of electron density to electron deficient but higher μ region in the process of backdonation. The differences in interaction energies (Table II) of the H_2 ligand with Pt cluster illustrate the important role of backdonation in σ-complex stabilization, where reduced backdonation results in less favorable interaction energy. The decomposition of MP2 interaction energy unraveled the exchange energy as the leading term being about twice greater than electrostatic or delocalization terms; there is also a significant contribution from the correlation component, which might be attributed to the rearrangements of charge density on Pt atoms. It is evident that both H–H bond breaking and stabilization of the σ-bond complex require sharing electrons with a vacant orbital associated with the Pt center as well as at least small backdonation.[57]

In the case of Pt_2H_{12} (but applies also to other clusters), the molecular-H_2 complex of metal hydride and the $Pt_2H_8(H_2)_2$ notation seems to be more proper. Besides $Pt_2H_8(H_2)_{n=1,2}$, the $Pt_4H_{16}(H_2)$ and $Pt_5H_{18}(H_2)_{n=1,2}$ clusters were obtained (data not included), where (H_2) denotes σ-bond complex of dihydrogen ligand. These σ-complexes were formed at sites on Pt atoms with Pt–H bond in *trans* position to H_2 ligand and exhibiting the lowest chemical potential. The H_2 molecules at sites with *trans* Pt–Pt bond with a little higher μ were found to be physisorbed. The synergis-

TABLE II. The PW91 interaction energy (ΔE) of Pt_2H_{n-2} with synergistically interacting H_2 molecule.

Cluster	ΔE (kcal/mol)	ΔE_{cc} (kcal/mol)[a]
Pt_2H_{10}	−15.49	−14.36
Pt_2H_{12}	−13.81	−12.58

[a]The counterpoise corrected interaction energy (Ref. 26).

TABLE III. The HOMO-LUMO orbital energies and energy gap of hydrogenated platinum clusters.

Cluster	E_{HOMO} (eV)	E_{LUMO} (eV)	$\Delta_{HOMO\text{-}LUMO}$ (eV)
Pt_2H_8	−7.2899	−4.1797	3.1103
Pt_2H_{10}	−7.2382	−3.5973	3.6382
Pt_2H_{12}	−7.1430	−3.0069	4.1361
Pt_3H_{12}	−7.3906	−4.3321	3.0586
Pt_4H_{16}	−7.1321	−4.8246	2.3075
Pt_5H_{20}	−6.7131	−3.9565	2.7565
Pt_7H_{28}	−6.7457	−4.5987	2.1470
Pt_8H_{30}	−5.8069	−4.2504	1.5538
Pt_9H_{34}	−6.2396	−4.4599	1.7769

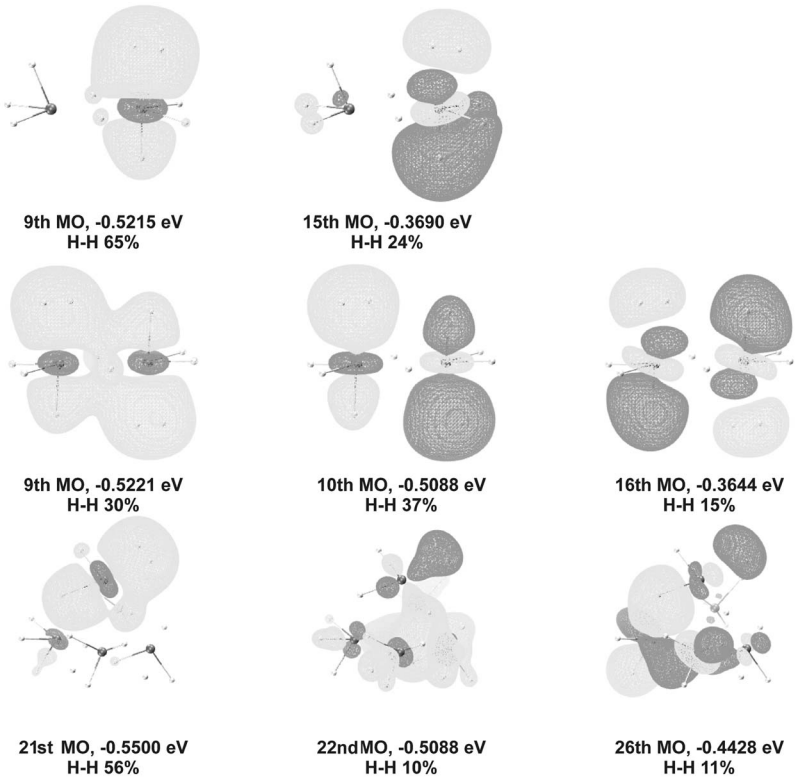

FIG. 7. Molecular orbitals with the greatest contribution to the H–H bond order. The orbital number and energy are followed by percentage contribution to H–H b_g. The first row shows MOs from Pt_2H_{10}, second Pt_2H_{12}, and last Pt_5H_{20} (all the valence MOs available in supporting data, Fig. S5).

tic (cooperative) H_2 coordination described here shows remarkable similar principles to the Dewar–Chatt–Duncanson model for olefin coordination.[57] The calculated lowering of H–H vibrational frequencies (3484–3570 versus 4386 cm^{-1} in isolated H_2) correlates with experimental[62] and theoretical findings[63] for such complexes. The intramolecular H–H stretching frequencies are smaller than those of physisorbed H_2 ($\sim$4200 cm^{-1} in Pt_4H_{20} or Pt_5H_{24}). Such sigma-bonded $Pt-H_2$ complexes (or Kubas interactions[57]) are desirable for fast kinetics due to intermediate binding energies between physisorption and chemisorption.

V. CONCLUSIONS

Reversible bonding of H_2 molecules in a similar fashion like O_2 to the heme group is desirable for hydrogen storing/operating materials. The primary advantage of such interaction is that each species can exist stably independently; thus association and dissociation energy barriers are quite low.[32] The σ-electron pair binds H_2 ligand to Pt by dative occupation of a vacant metal orbital.[57] The σ-complex has to be stabilized by backdonation, which results in a stronger interaction than physisorption or hydrogen bonding. H_2 is found to be a strong π-acceptor; thus σ-complex might easily transform into hydride. Shearing only σ-electron pair is not enough to break the H–H bond, and it is the accompanying overpopulation of dihydride σ^* orbital that leads to the cleavage of hydrogen molecule[57] due to the strengthening of the Pt–H interaction. The unique feature of H_2 is that it has just one σ-bonding electron pair; thus σ-bond complex strongly activates dihydrogen, which binds symmetrically, always side-on to the metal. The *trans* ligand has great influence on $Pt-H_2$ binding nature and strength; particularly a hydride ligand weakens the interaction compared to Pt species in *trans* ligand position.

The corresponding interactions are well known and described in literature,[43,57] particularly as a part of catalytic hydrogenation cycle. We were able to visualize the reactive regions of Pt clusters using electronic chemical potential calculated by the RDFT method. Regions of low electronic chemical potential were recognized as electrophilic centers characterized by electron withdrawing tensile stress. Through a screen of chemical potential of other materials, it is possible to quickly determine species able to reverse the binding of molecular hydrogen with moderate strengths. Covalent binding of H atoms to Pt significantly lowered electronic chemical potential in *trans* position to Pt–H bond. The relevant regions appeared only in small clusters. The σ-bonding of H_2 stabilizes both $Pt-H_2$ and *trans* Pt–H bond.

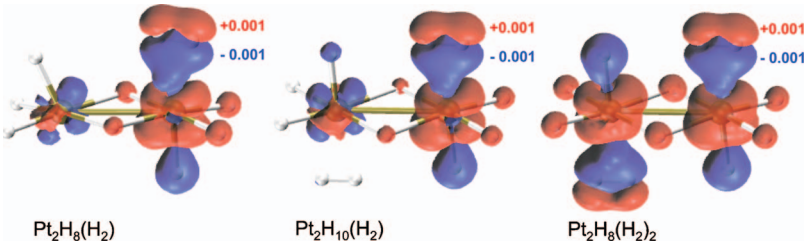

FIG. 8. (Color) The interaction energy density of Pt_2H_8 and H_2 in the Pt_2H_{10} cluster $[Pt_2H_8(H_2)]$, Pt_2H_{10} and H_2 in the Pt_2H_{12} cluster $[Pt_2H_{10}(H_2)]$, and Pt_2H_8 and two H_2 in the Pt_2H_{12} cluster $[Pt_2H_8(H_2)_2]$.

In large clusters surface Pt atoms do not expose to the molecular surface vacant orbitals with sufficiently low chemical potential to constitute a stable σ-bond complex with H_2 due to Pt atom occupying *trans* ligand position. We anticipate that bulk Pt materials are not able to stabilize the σ-complex. The b_ε- and b_μ-bond orders picture an energetical characteristic of bonding electrons. The Pt–Pt bond's average strength decrease with increasing cluster size and occupancy with hydrogen, and the bigger clusters also have weaker terminal Pt–H bonds and stronger $3c/2e$ interactions. The dihydrogen ligand H–H b_ε-bond order was higher than any geminal or vicinal Pt–H bond, while the b_μ index was similar to that of $3c/2e$ Pt–H–Pt bridge bonds. The similarity of μ for Pt–Pt and H–H bonds encourages H atoms to occupy the bridging position. Involvement of $\sigma_{PtH}{}^*$ and σ_{PtH} orbitals in donor-acceptor interactions leads to stronger bonding than engaging $\sigma_{PtH}{}^*$ and Pt lone pair.

ACKNOWLEDGMENTS

This research was supported by Japanese Government MEXT scholarship through Kyoto University.

[1] Basic Research Needs for the Hydrogen Economy, www.science.doe.gov/bes/Hydrogen.pdf.
[2] L. Schlapbach and A. Zuttel, Nature (London) **414**, 353 (2001).
[3] R. Coontz and B. Hanson, Science **305**, 957 (2004).
[4] M. Fichtner, Adv. Eng. Mater. **7**, 443 (2005).
[5] L. Gagliardi and P. Pyykko, J. Am. Chem. Soc. **126**, 15014 (2004).
[6] B. Bogdanovic, M. Felderhoff, A. Pommerin, T. Schuth, and N. Spielkamp, Adv. Mater. (Weinheim, Ger.) **18**, 1198 (2006).
[7] W.-Q. Deng, X. Xu, and W. A. Goddard, Phys. Rev. Lett. **92**, 166103 (2004).
[8] T. Yildirim and S. Ciraci, Phys. Rev. Lett. **94**, 175501 (2005).
[9] Q. Sun, P. Jena, Q. Wang, and M. Marquez, J. Am. Chem. Soc. **128**, 9741 (2006).
[10] T. Yildirim and M. R. Hartman, Phys. Rev. Lett. **95**, 215504 (2005).
[11] A. Tachibana, Theor. Chem. Acc. **102**, 188 (1999).
[12] A. Tachibana, J. Chem. Phys. **115**, 3497 (2001).
[13] A. Tachibana, in *Stress Induced Phenomena in Metallization*, edited by S. P. Baker (American Institute of Physics, New York, 2002), pp. 205–211.
[14] A. Tachibana, in *Reviews in Modern Quantum Chemistry: A Celebration of the Contributions of Robert Parr*, edited by K. D. Sen (World Scientific, Singapore, 2002), Vol. 2, pp. 1327–1366.
[15] A. Tachibana, in *Fundamental Perspectives in Quantum Chemistry: A Tribute to the Memory of Per-Olov Löwdin*, edited by E. Brändas and E. Kryachko (Kluwer, Dordrecht, 2003), Vol. 2, pp. 211–239.
[16] A. Tachibana, Int. J. Quantum Chem. **100**, 981 (2004).
[17] A. Tachibana, J. Mol. Model. **11**, 301 (2005).
[18] A. Tachibana and R. G. Parr, Int. J. Quantum Chem. **41**, 527 (1992).
[19] A. Tachibana, Int. J. Quantum Chem., Quantum Chem. Symp. **32**, 181 (1987).
[20] P. Szarek, Y. Sueda, and A. Tachibana, J. Chem. Phys. **129**, 094102 (2008).
[21] A. Tachibana, Int. J. Quantum Chem. **57**, 423 (1996).
[22] A. Tachibana, K. Nakamura, K. Sakata, and T. Morisaki, Int. J. Quantum Chem. **74**, 669 (1999).
[23] P. Szarek and A. Tachibana, J. Mol. Model. **13**, 651 (2007).
[24] R. T. Sanderson, Science **114**, 670 (1951).
[25] E. Wigner and J. Bardeen, Phys. Rev. **48**, 84 (1935).
[26] J. Bardeen, Phys. Rev. **49**, 653 (1936).
[27] L. Onsager, Phys. Rev. **37**, 405 (1931).
[28] L. Onsager, Phys. Rev. **38**, 2265 (1931).
[29] A. Tachibana, J. Math. Chem. **7**, 95 (1991).
[30] W. A. Sokalski, S. Roszak, and K. Pecul, Chem. Phys. Lett. **153**, 153 (1988).
[31] S. F. Boys and F. Bernardi, Mol. Phys. **19**, 553 (1970).
[32] C. Zhou, J. Wu, A. Nie, R. C. Forrey, A. Tachibana, and H. Cheng, J. Phys. Chem. C **111**, 12773 (2007).
[33] M. J. Frisch, G. W. Trucks, H. B. Schlegel *et al.*, GAUSSIAN 03, Revision C.02, Gaussian, Inc., Wallingford, CT, 2003.
[34] J. P. Perdew and Y. Wang, Phys. Rev. B **45**, 13244 (1992).
[35] P. J. Hay and W. R. Wadt, J. Chem. Phys. **82**, 299 (1985).
[36] W. J. Hehre, R. Ditchfield, and J. A. Pople, J. Chem. Phys. **56**, 2257 (1972).
[37] M. S. Gordon, Chem. Phys. Lett. **76**, 163 (1980).
[38] B. Delley, J. Chem. Phys. **92**, 508 (1990).
[39] C. W. Bock and M. Trachtman, J. Phys. Chem. **98**, 95 (1994).
[40] H. Guo and M. Karplus, J. Chem. Phys. **91**, 1719 (1989).
[41] J. A. Sordo, Chem. Phys. Lett. **316**, 167 (2000).
[42] A. A. Merkulov, P. Mountford, and G. I. Nikonov, in *Organosilicon Chemistry V: From Molecules to Materials*, edited by N. Auner and J. Weiss (Wiley-VCH, New York, 2003), pp. 451–455.
[43] A. Dedieu, Chem. Rev. (Washington, D.C.) **100**, 543 (2000).
[44] K. Doi, P. Szarek, K. Nakamura, M. Senami, and A. Tachibana, Regional DFT Program Package, Ver. 2, Tachibana Laboratory, Kyoto University, Kyoto, 2007.
[45] W. L. DeLano, DeLano Scientific LLC, San Carlos, CA (http://www.pymol.org).
[46] W. Humphrey, A. Dalke, and K. Schulten, J. Mol. Graphics **14**, 33 (1996).
[47] See EPAPS Document No. E-JCPSA6-130-023905 for Fig. S1 [change in energy density ($b\varepsilon$) and chemical potential ($b\mu$) bond orders and NBO bond orders with bond length for structures of (a) optimized in GAUSSIAN 03 and of (b) in DMOL3 (Ref. 32) program packages (details in text)], Fig. S2 (structures, atom numbering, and bonding pattern in Pt clusters), Fig. S3 (the largest eigenvalue of electronic stress tensor), Fig. S4 (chemical potential on the interface surface of bare Pt clusters), Fig. S5 (the valence molecular orbitals of Pt_2H_8, Pt_2H_{10}, and Pt_2H_{12} clusters), and Table S1 [Lagrange point data (GAUSSIAN 03: PW91PW91/6-31G**, LanL2DZ optimized structures)]. For more information on EPAPS, see http://www.aip.org/pubservs/epaps.html.
[48] A. E. Reed and F. Weinhold, J. Chem. Phys. **78**, 4066 (1983).
[49] A. E. Reed, R. B. Weinstock, and F. Weinhold, J. Chem. Phys. **83**, 735 (1985).
[50] L. S. Bartell and B. L. Carrol, J. Chem. Phys. **42**, 1135 (1965).
[51] C. G. Van de Walle, P. J. H. Denteneer, Y. Bar-Yam, and S. T. Pantelides, Phys. Rev. B **39**, 10791 (1989).
[52] P. E. Blöchl, Phys. Rev. B **62**, 6158 (2000).
[53] J. Kang, E.-C. Lee, K. J. Chang, and Y.-G. Jin, Appl. Phys. Lett. **84**, 3894 (2004).
[54] R. Bau, M. H. Drabnis, L. Garlaschelli, W. T. Klooster, Z. Xie, T. F. Koetzle, and S. Martinengo, Science **275**, 1099 (1997).
[55] A. Janotti and C. G. Van de Walle, Nature (London) **6**, 44 (2007).
[56] Q. Cui, D. G. Musaeev, and K. Morokuma, J. Chem. Phys. **108**, 8418 (1998).
[57] G. J. Kubas, J. Organomet. Chem. **635**, 37 (2001), and references cited therein.
[58] M. Brookhart, M. L. H. Green, and G. Parkin, Proc. Natl. Acad. Sci. U.S.A. **104**, 6908 (2007).
[59] M. Brookhart and M. L. H. Green, J. Organomet. Chem. **250**, 395 (1983).
[60] S. J. La Placa and J. A. Ibers, Inorg. Chem. **4**, 778 (1965).
[61] T. Koopmans, Physica (Amsterdam) **1**, 104 (1934).
[62] R. A. Henderson, Transition Met. Chem. **13**, 474 (1988), and references cited therein.
[63] J. Íñiguez, W. Zhou, and T. Yildirim, Chem. Phys. Lett. **444**, 140 (2007).